PCCP

Accepted Manuscript

ROYAL SOCIETY OF CHEMISTRY

www.rsc.org/pccp

Comparative kinetic and energetic modelling of phyllosemiquinone oxidation in Photosystem I.

Stefano Santabarbara[1 *] and Giuseppe Zucchelli[1].

[1]Istituto di Biofisica, Consiglio Nazionale delle Ricerche, Via Celoria 26, 20133 Milano, Italy.

Keywords: Photosystem I, Electron Transfer, Phylloquinone, Energetics, Tunnelling.

List of abbreviation: PS I: Photosystem I; RC, Reaction Centre; ET, Electron Transfer; $PhQ^{(-)}_{(A/B)}$ phyllo(semi)quinone; $F^{(-)}_{X}$ iron-sulphur cluster X (reduced); $F_{A/B}$ iron-sulphur clusters A and B.

[*]**To whom correspondence should be addressed:** Stefano Santabarbara, Istituto di Biofisica, Consiglio Nazionale delle Ricerche, Via Celoria 26, 20133 Milano, Italy. Tel: +39 02 503 14857. e-mail: stefano.santabarbara@cnr.it

Abstract.

The oxidation kinetics of phyllo(semi)quinone (PhQ), that acts as an electron transfer (ET) intermediate in the Photosystem I reaction centre, are described by a minimum of two exponential phases, characterised by lifetimes in the 10-30 ns and 150-300 ns intervals. The fastest phase is considered to be dominated by the oxidation of the PhQ molecule coordinated by the PsaB reaction centre subunit (PhQ_B), and the slowest one by the oxidation of the PsaA coordinated PhQ (PhQ_A). Testing different energetic schemes within an unified theory-based kinetic modelling approach, provides reliable limit-values for some of the physical-chemical parameters controlling these ET reactions: i) the value of ΔG^0 associated with PhQ_A oxidation is smaller than ~ +30 meV; ii) the value of the total reorganisation energy (λ_t) likely exceeds 0.7 eV; iii) different mean nuclear modes are coupled to PhQ_B and PhQ_A oxidation, the former being larger, and both being $\geq$ 100 cm^{-1}.

Electron transfer (ET) reactions are the foundations of several key metabolic processes, amongst which the most intensively investigated are oxidative respiration and photosynthesis. In these processes, electron transfer take places through hierarchically organised cofactors chains, coordinated by multi-subunits protein complexes. The nature of the redox active prosthetic groups encounter in Nature is relatively limited. Therefore, proteins play an important role in controlling the physical-chemical properties of the bound cofactors, allowing efficient electron transfer to occur over a wide range of distances and electro-chemical potential ranges. Amongst the most efficient ET processes occurring in biology are the light-induced reactions in photosynthetic reaction centres, which are known to take place with quantum yields approaching unity.

Phylloquinones (PhQ) act as electron transfer intermediates in the electron transfer chains of Photosystem I (PSI) [1-5 and refs. therein]. The overall oxidation kinetics of semi-phylloquinone by the next electron acceptor, the iron-sulphur cluster F_X, is multiphasic and, at room temperature, it is characterized by two dominant lifetimes in the 10-30 ns and 250-350 ns ranges[1-5]. The two putative electron transfer chains present in the PSI reaction centre are both active in electron transfer reactions, according to the bidirectional electron transfer model [e.g. 1-11]. Spectroscopic investigations combined to site-selected mutagenesis of the PhQ^- binding niches of the two principal reaction centres subunits, PsaA and PsaB, indicate that the fastest kinetic component (10-30 ns) is dominated by the oxidation of the PhQ^- cofactor coordinated primarily by PsaB (designed as A_{1B} or PhQ_B), whereas the slowest phase reflects the oxidation of PhQ^- coordinated by the PsaA subunit[1-5, 8] (A_{1A} or PhQ_A). The lifetimes also display markedly different temperature dependences[12-15]. The fast phase is weakly activated, with apparent activation barrier in the 7-43 meV range[12-15]. The slowest phase shows a more pronounced temperature dependence, in the 100-130 meV range[14, 15]. The structural models[16, 17] indicate similar arrangements of the PhQ_A or PhQ_B cofactors with respect to the electron acceptor F_X that is shared by the two electron transfer chains. Subtle differences in the coordination and orientation of the PhQ_A or PhQ_B moieties within the reaction centre might be present, as recently suggested[18]. However, these are not sufficient to explain the one order of magnitude difference in the reported lifetimes. Hence, the kinetic observations have been taken

as an indication of asymmetries in the physical-chemical properties of these cofactors induced by protein-cofactor interactions[1-5]. Different approaches, relying either on structure-based quantum-chemical and semi-classical computational methods[19-21] or on the analysis and modelling of the experimental kinetics[1, 14, 22], have been employed to address this issue.

A considerable range of the standard redox potentials (E^0) of the PhQ_B^-/PhQ_B and PhQ_A^-/PhQ_A couples has been reported from structure-based computational methods [e.g. 19-21]. From this spread of midpoint potentials, the standard free energy differences for PhQ_A^- oxidation by F_X ($\Delta G^0_{PhQ_A \to F_X}$) range from –85, which is largely exergonic[21], to + 175 meV, which is largely endergonic instead[19]. The oxidation of PhQ_B^- by F_X is generally considered to be thermodynamically favourable. However, even the estimate of the free energy coupled to PhQ_B^- oxidation ($\Delta G^0_{PhQ_B \to F_X}$) varies considerably, ranging from –250 meV[21], i.e. a largely exergonic reaction, to the –40 - +20 meV range[19], i.e. a weakly exer- to ender-gonic reaction. As discussed by Karyagina *et al.*[20] and more extensively by Ptushenko *et al.*[21], the computed values depend on the protein volume taken into account, the number of crystallographic water molecules in the vicinity of the PhQ molecule and the approach chosen to describe the dielectric properties of the protein medium.

Estimation of the E^0 values of PhQ_A^-/PhQ_A ($E^0_{PhQ_A}$) retrieved from experimental data also display a significant spread, ranging from ~ –800 to –530 mV (reviewed in refs. **1, 2, 12, 23**). Considering the values reported for the F_X redox potential, $-730 < E^0_{F_X} < -630$ mV [1, 3, 12, 23-25], this makes PhQ_A^- oxidation from largely endergonic to substantial exergonic, i.e. $\sim -100 < \Delta G^0_{PhQ_A \to F_X} < +100$ meV. This range of values is comparable to that obtained from structure-based computational studies. With the exception of a single report in which a direct titration of PhQ_A^- was claimed[26], in all other cases the $E^0_{PhQ_A}$ values were extrapolated from applying theories at various level of sophistication to kinetic data[1, 12, 14, 22, 27]. It is worth noticing that the value obtained from the direct electrochemical titration ($E^0_{PhQ_A} = -530$ mV)[26] falls on the more electro-positive edge of the potential spread.

Hence, whereas there is a general agreement in considering that PhQ_B^- oxidation is largely favourable from a thermodynamic point of view and $\Delta G^0_{PhQ_B \rightarrow F_X} \leq$ –50 meV, the energetic parameters associated to PhQ_A^- oxidation are much less clear-cut. Suggestions from the literature can be grouped in three possible energetic scenarios:

i) largely energetically unfavourable ("large uphill"), i.e. $\Delta G^0_{PhQ_A \rightarrow F_X} \geq$ +75 meV, equivalent to ~3 k_BT at room temperature [19, 20];

ii) associated to a weak driving force, i.e. $-40 \leq \Delta G^0_{PhQ_A \rightarrow F_X} \leq +40$ meV [1, 20, 22, 23];

iii) largely energetically favourable, i.e. $\Delta G^0_{PhQ_A \rightarrow F_X} \leq -75$ meV [21, 27].

Theory-based kinetic modelling of PhQ^- oxidation were interpreted in favour of the "weak driving force" hypothesis[1]. However, since these calculations were performed, a substantial amount of novel information has been acquired, both from computational and experimental approaches (e.g. ref **3, 5** and reference therein and refs. **28-33**). Although both computational and theory-based kinetic modelling approaches require the choice of parameters not readily accessible in the experiments, the "weak driving force" hypothesis has proven to be rather robust as it allowed to describe the effect of several mutants of PhQ^- binding niche, including some which were produced successively[28-30], as well as experiments involving PhQ substitution with artificial quinone analogues[32-36].

Recently, Mula *et al.*[31] performed a detailed re-investigation of the PhQ^- oxidation temperature dependence including molecular dynamics calculations. They suggested that, beside the value of ΔG^0, a large difference in the angular frequency ($\bar{\omega}$) of the mean nuclear mode coupled to PhQ_A^- and PhQ_B^- oxidation ($\bar{\omega}_{PhQ_A \rightarrow F_X}$ = 173 and $\bar{\omega}_{PhQ_B \rightarrow F_X}$ = 378 cm^{-1}, respectively) is responsible for the one order of magnitude faster oxidation of PsaB coordinated redox moiety. Moreover, these authors reported the full set of parameters which is required to describe the temperature dependence of the electron transfer rate constants, in terms of nuclear mediated electron transfer theory[37-39]. Although in their study the values of ΔG^0 were

not tabulated[31], these can be retrieved from the reported activation energies (ΔG^*), which was, for PhQ_A^- oxidation, 243 meV [31]. From this value, $\Delta G^0_{PhQ_A \rightarrow F_X}$ = +125 meV (*vide infra*), that fall in the large energetically uphill scenario.

Uncovering the factors controlling ET reactions in photosynthetic RC is of central importance both under biological and biotechnological perspective. In fact, the extremely high efficiency of light conversions in these complex cofactor-protein systems makes them ideal models to study these processes and to design artificial and hybrid photovoltaic devices.

Therefore, in order to obtain a better understanding of the energetics associated with PhQ^- oxidation in PSI, and in an attempt to derive a unifying view of these ET reactions, the different models advanced in the literature are here investigated by comparative kinetic modelling. The theoretical framework for the description of electron transfer rates introduced by Hopfield[38, 39], which considers explicitly a single (mean) nuclear mode coupled to the ET reactions, has been employed. The consistency of the thermodynamic scenarios was compared with the experimental PhQ^- oxidation kinetics detected both at room temperature and in the 180-320 K temperature interval.

We conclude that both the "weak driving force" and the "large driving force" energetic scenarios are compatible with the experimental results. The "large uphill" energetic is not compatible with the experiments instead.

Experimental procedures

Theoretical considerations.

Kinetic modelling. The kinetics of PhQ^- oxidation was modelled in terms of the reaction scheme of Figure 1: the oxidation of PhQ_A^- by F_X, is described by the rate constants k_1 and k_{-1}; the oxidation of PhQ_B^- by F_X, is described by the rate constants k_2 and k_{-2}; the oxidation of the reduced form of F_X (F_X^-) by the terminal electron acceptors, the iron-sulphur clusters F_A and F_B, is described by the rate constant k_3, which represent an (irreversible) output from the system.

The system of ordinary differential equation (ODE) associated to the kinetic scheme of Figure 1 is:

$$\begin{cases} \dfrac{d\mathrm{PhQ_A}(t)}{dt} = -k_1\mathrm{PhQ_A}(t) + k_{-1}\mathrm{F_X}(t) \\ \dfrac{d\mathrm{PhQ_B}(t)}{dt} = -k_2\mathrm{PhQ_B}(t) + k_{-2}\mathrm{F_X}(t) \\ \dfrac{d\mathrm{F_X}(t)}{dt} = -(k_{-1}+k_{-2}+k_3)\mathrm{F_X}(t) + k_1\mathrm{PhQ_A}(t) + k_2\mathrm{PhQ_B}(t) \end{cases} \quad \text{Eqn. 1}$$

This can be written in matrix form as $\dot{\mathbf{S}} = \mathbf{K}\cdot\mathbf{S}$, where $\mathbf{S}$ and $\dot{\mathbf{S}}$ are column vectors which have as elements the population evolutions of each cofactor and their first derivative with respect to time, respectively. $\mathbf{K}$ is a square matrix having as its elements the rate constants, as detailed in equation 1.

The system in equation 1 has general solutions of the form:

$$\mathbf{S} = \sum_{i=1}^{3} c_i \cdot \mathbf{V}_i \cdot e^{\gamma_i t} \quad \text{Eqn. 2}$$

where $\mathbf{V_i}$ is the *i*-th eigenvector of matrix $\mathbf{K}$ and γ_i is the *i*-th eigenvalue. The constants c_i depend on the initial conditions ($\mathbf{S}_{t\to 0}$). The eigenvalues are related to the experimental lifetime values (τ_i) through $\tau_i = -\gamma_i^{-1}$, and are unambiguously determined once the rate constants which compose the matrix $\mathbf{K}$ are established. The eigenvectors are related to the experimental pre-exponential amplitudes in a less direct fashion. The elements of $\mathbf{V_i}$ are not accessed directly in the experiments, it is only their sum, weighted by the spectroscopic properties of the cofactor, that it is observed. Although the amplitudes will not be discussed in great details in this study, we take the assumption, which is well substantiated by experimental evidences [e.g. 12, 25], that the spectroscopic signature of $\mathrm{F_X}$ can be considered negligible whereas that of $\mathrm{PhQ_A^-}$ and $\mathrm{PhQ_B^-}$ are dominant and equivalent, i.e. that $\varepsilon_{\mathrm{PhQ_A}} = \varepsilon_{\mathrm{PhQ_B}} >> \varepsilon_{\mathrm{F_X}}$, where ε is the extinction coefficient. Moreover, the eigenvectors depend on the boundary conditions which, in this case, are considered as the relative molar fractions at time t=0. We took $\mathrm{PhQ_A^-}(0) = \mathrm{PhQ_B^-}(0) = 0.5$ and $\mathrm{F_X^-}(0) = 0$, i.e. equal initial population stemming from symmetric statistical utilisation of the two electron transfer branches.

The exact utilisation of the two branches in PSI is still a matter of controversy. A rather broad range of figures, ranging from 0.5:0.5 to 0.8:0.2, in favour of the ET chain primarily coordinated by the PsaA subunit, is reported in the literature [1-5, 40-44]. These values depend also on the organism from which PS I was purified or studied [e.g. 40-44]. Since we aim for a semi-quantitative description of the experimental evidence, and since we focus primarily on the decay lifetimes, the approximation $\mathrm{PhQ}_{\mathrm{A}}^{-}(0) = \mathrm{PhQ}_{\mathrm{B}}^{-}(0) = 0.5$ does not significantly affect any of the conclusions.

Electron Transfer Rate Constants. The values of the electron transfer rate constants, which are the elements of matrix $\mathbf{K}$, were calculated using the approach introduced by Hopfield[39] when considering a mean nuclear mode coupled to the electron donor, *D*, and the acceptor, *A*. The rate of electron transfer between a donor-acceptor pair, $k_{D\to A}$, is then described by:

$$k_{D\to A} = \frac{2\pi}{\hbar}\left|H_{DA}\right|^2 \cdot f(T) \qquad \text{Eqn. 3}$$

where $\hbar$ is the Dirac constant, $|H_{DA}|$ is the electronic coupling element of the Hamiltonian. The temperature-dependent Franck-Condon factors are described by the $f(T)$ function:

$$f(T) = \frac{1}{\sqrt{2\pi}\sigma(T)} e^{-\frac{(\Delta G^0 + \lambda_t)^2}{2\sigma(T)^2}} \qquad \text{Eqn. 4}$$

where, ΔG^0 is the standard Gibbs free energy difference and λ_t, the total reorganisation energy. The standard conditions, refer to atmospheric pressure and equal molar fractions of (reduced) donor and (oxidised) acceptors. These conditions are often encountered in RC when considering suitable initial conditions, *i.e.* at a given time following the light excitation. PhQs are reduced in less than 50 ps [1-5] and are oxidised in 10-300 ns, as discussed above. This guarantees that the standard conditions are fulfilled. As discussed by Hopfield[39], it is possible to assume to a very good approximation that contribution of entropy change to the free energy are absent or negligible for tunnelling-mediated ET reactions between a Donor-Acceptor

cofactors pair bound to a protein matrix. Therefore, the value of ΔG^0 (which would be equivalent to that of an enthalpy/internal energy change) can be considered as temperature-independent. The variance, σ^2, is described by:

$$\sigma^2 = \lambda_t \hbar\bar{\omega} \cdot \coth \frac{\hbar\bar{\omega}}{2k_B T}, \qquad \text{Eqn. 5}$$

where, k_B is the Boltzmann constant, and $\bar{\omega}$ is the (angular) frequency of the mean nuclear mode coupled to electron transfer. This term accounts for the temperature dependence of the ET reaction. When $2k_B T >> \hbar\bar{\omega}$, equation 5 reduces to:

$$\sigma^2 = 2\lambda_t k_B T \qquad \text{Eqn. 6}$$

that, substituted into Equations 3 and 4 yields the formula derived by Marcus [37, 38]:

$$k_{D\to A} = \frac{2\pi}{\hbar} \frac{\left|H_{DA}\right|^2}{\sqrt{4\pi\lambda_t k_B T}} e^{-\frac{(\Delta G^0 + \lambda_t)^2}{4\lambda_t k_B T}} \qquad \text{Eqn. 7}$$

By analogy with the classical Arrhenius treatment of the reaction rate temperature dependence, the argument of the exponential of Equation 7 is the activation energy, ΔG^*, divided by $k_B T$:

$$\Delta G^* = \frac{(\Delta G^0 + \lambda_t)^2}{4\lambda_t} \qquad \text{Eqn. 8}$$

It is emphasized that Equation 8 is valid only under the $2k_B T >> \hbar\bar{\omega}$ conditions, which are attained if T is sufficiently high (so-called high temperature approximation), and/or when $\bar{\omega}$ is a mode of sufficient low frequency with respect to $k_B T$.

Choice of Parameter Sets. Using the described formalism, the rate constants composing the matrix **K** depend on a limited set of parameters: i) the standard free, $\Delta G^0_{D\to A}$, and reorganisation energies, $\lambda_{t,D\to A}$; ii) the mean frequency of nuclear mode coupled to electron transfer $\overline{\omega}_{D\to A}$; iii) the value of electronic coupling element $|H_{DA}|$; where the $D\to A$ subscript indicate a specific donor-acceptor pair. Seldom the values for all these parameters have been estimated in a single study. The most complete set for both the $PhQ^-_A \to F_X$ and $PhQ^-_B \to F_X$ reactions was reported by Mula *et al.* [31]. They gave values for $\lambda_{t,D\to A}$, $|H_{DA}|^2$ and $\Delta G^*_{D\to A}$, from which, using Eqn.8, $\Delta G^0_{D\to A}$ can be computed (see discussion below and Table 1). The value $\lambda_{t,D\to A}$ = 0.7 eV was assumed by these authors for both PhQ^- oxidation reactions. Similar values were also utilised in previous kinetic modelling studies [1, 22, 28, 29]. On the other hand, the set of parameters associated to the $F^-_X \to F_{A/B}$ reaction was not presented.

The values of $\Delta G^0_{D\to A}$ have been estimated in several studies and by a range of approaches (for compilations of values see [1, 3, 12, 19-27]). Whereas there is a general agreement that $\Delta G^0_{F_x\to F_{A/B}} < -100$ meV (reviewed in **1, 3, 12**), a substantial spread of value $\Delta G^0_{PhQ\to F_X}$ ($\cong \pm 200$ meV) has been reported[1, 3, 12, 19-31, 45]. Therefore the energetic associated PhQ^- oxidation still present considerable margin of uncertainty. This spread of values depends, partially, on the strategy employed to retrieve the redox potentials and free energy difference. For instance, the protonation state of individual protein residues and the effect of protein and water molecules were taken into account *explicitly* in electrostatic computations [19-21]. Yet the results obtained in the different studies are not univocal. Instead, when the parameters are retrieved from the analysis of spectroscopic data, residues protonation states, and solvent effects are considered macroscopically. Therefore, operational, *effective*, values, in which the microscopic contribution can not be disentangled, are obtained instead. In the present modelling study we have used the latter approach and, therefore, the values of ΔG^0 should be considered as effective ones. However, the parameter values proposed from studies in which protonation state and solvation effects, including the effect of bound water,

were considered explicitly, have been also considered performing comparative kinetic simulations.

Therefore, using a minimal kinetic modelling scheme, different energetic scenario stemming from literature reports, are tested by comparison with the experimental results. Some representative values taken from previous investigation and which are used in the present kinetic modelling study are reported in Table 1.

The other parameters, unless specifically stated, are assumed to have the same value for all of the three electron transfer reactions considered. For the total reorganisation energy we considered $0.5 < \lambda_t < 1$ eV, an interval covering the most probable values retrieved from a survey of electron transfer reactions in redox-active enzymes[46, 47]. The extreme values of λ_t are close to either the estimate of λ_t for P_{700}^{+} reduction by plastocyanin[15, 48] or the highest bound of PhQ_A^- oxidation by F_X^- [13, 14]. For the energy of the mean nuclear mode we have considered values in the range of $2.5 < \hbar\bar{\omega} < 34$ meV (i.e. 20-274 cm^{-1}). The highest bound is the average of the values reported by Mula *et al.*[31] whereas the lowest bound represents a "soft" mode which closely approaches the high-temperature approximation (Eqn. 7).

The strength of the electronic coupling element $\left|H_{DA}\right|^2$ was estimated using the approximated expression [38, 39, 46, 47]:

$$\left|H_{DA}\right|^2 = \left|H_{DA}^0\right|^2 \cdot \exp(-\beta \cdot R_{DA}) \qquad \text{Eqn. 9.}$$

where R_{DA} is the donor-accepted edge-to-edge distance (corrected for the van der Waals radii), β is a medium-depended damping factor, and $\left|H_{DA}^0\right|$ is the maximal value attained at full electronic wave function overlap. R_{DA} is derived from the crystallographic structural model (pdb entry: 1JB0[16]), an average value of $\beta = 1.34$ $Å^{-1}$ was estimated in electron transfer proteins [e.g. 22, 46, 47] and a reasonable value for $\left|H_{DA}^0\right|^2$ is ~$1 \cdot 10^{-3}$ eV^2 [33, 34, 46, 47].

Computations. Kinetic modelling was performed using the Maple 9 (MapleSoft, Waterloo, Ontario, Canada).

Results and Discussion.

Kinetic modelling of PhQ^- *oxidation reduction at room temperature.*

In order to compare how the midpoint potential estimates for the PhQ_A^- / PhQ_A and PhQ_B^- / PhQ_B redox pairs, retrieved from different analytical approaches, reflect on the description of the kinetic of PhQ^- oxidation at room temperature, some of the most representative values for the different scenarios previously reported in the literature were considered, within the kinetic modelling framework described above.

Large uphill PhQ_A^- *oxidation.* Sets of parameter at different level of detail have been presented in previous investigations [e.g. 1, 12-14, 19-22]. We use, as a starting point, the comprehensive estimates given by Mula and coworkers [31] (and Table 1) for $\lambda_{t,D\to A}$, $\bar{\omega}_{D\to A}$, $\Delta G^*_{D\to A}$ and $|H_{DA}|^2$, which were obtained from the fitting of the PhQ^- oxidation lifetimes temperature dependences in terms of Eqns. 3-5. From the reported values of $\Delta G^*_{D\to A}$, those of $\Delta G^0_{D\to A}$ can be calculated using Eqn.8 considering that $\lambda_{t,D\to A}$ was set at 0.7 eV by their study. This, however, involves the solution of a second order equation, from which two possible values of $\Delta G^0_{D\to A}$ are obtained. We have chosen $\Delta G^0_{PhQ_A\to F_X}$ = +125 meV and $\Delta G^0_{PhQ_B\to F_X}$ = –58 meV as the complementary solutions are, in both cases, unrealistic. In fact, they exceed the value of –1 eV, which would put both phylloquinones E^0 well above the absorbed photon energy corresponding to the excited state of PSI photochemical reaction centre*.

Mula and coworkers did not report the set of parameters associated with $F_X^- \to F_{A/B}$ electron transfer, as this reaction was not investigated directly in their study[31]. Since these parameters are needed for the present modelling, and in order to limit the number of adjustable parameters, we have considered $\lambda_{t,F_X\to F_{A/B}} = \lambda_{t,PhQ\to F_X}$, i.e. 0.7 eV. Unless otherwise specified, we will assume the same value of λ_t for all the reactions considered. The same approach will be adopted for the values of $\bar{\omega}_{D\to A}$.

* Considering a larger value of the reorganisation energy, such as λ_t=1, the calculated value of $\Delta G^0_{PhQ_B\to F_X}$ becomes –230 meV and that of $\Delta G^0_{PhQ_A\to F_X}$ becomes –15 meV. The latter value falls in what is here defined as "weak" driving force scenario for PhQ_A^- oxidation, which is discussed further on in the text

Nonetheless, since different values for $\bar{\omega}_{PhQ_A \to F_X}$ = 173 cm^{-1} and $\bar{\omega}_{PhQ_B \to F_X}$ = 378 cm^{-1} were reported[31], an intermediate value for $\bar{\omega}_{F_X \to F_A}$ of 275 cm^{-1} was considered. The value of the free energy difference $\Delta G^0_{F_X \to F_{A/B}}$ was set at –150 meV. This approaches the average of the difference between the reported midpoint potentials of F_X and F_A (as compiled in refs. **1, 3, 12**). Moreover, F_A and F_B are almost iso-potential. Simulation for $\Delta G^0_{F_X \to F_{A/B}}$ = –106 meV, which allows direct comparison with the calculated potential reported by Ptushenko and coworkers[21], are presented in the Supplementary information (Figure S1).

The kinetic simulations performed using the above discussed parameters are presented in Figure 2 (panel A) and the parameters describing the cofactors temporal evolution are listed in Table 2. In order to compare the simulated kinetics with the experimental results it is necessary to consider that, due to the low value of $\Delta\varepsilon_{F_X}$, it is $\Delta\varepsilon_{PhQ}$ which dominates the experimental kinetics. Moreover, since PhQ_A^- and PhQ_B^- can not be monitored individually, the closest representation of the experiments is provided by the sum of the individual semiquinone relaxation kinetics. Hence, although the temporal evolution of the each considered cofactor is computed (and shown in Figure 2), it is the "overall" $PhQ^-(t) = PhQ_A^-(t) + PhQ_B^-(t)$ population relaxation that has to be compared with the experiments.

For the just discussed energetic scenario ("large uphill PhQ_A^- oxidation"), the overall PhQ^- oxidation extends for over 20 μs (Figure 2A), whereas it is completely relaxed after ~1–1.5 μs according to the experimental data[1-4]. The simulated kinetics are described by three lifetimes of 2.6 ns, 10 ns, 9.6 μs with associated amplitudes of 0.18, -0.16, 0.97, respectively (Table 2). The two faster lifetimes fall on the lower range of values (faster decay) reported in the experiments, which are more frequently observed in PSI isolated from cyanobacteria [e.g. 1-3, 12, 31, 40, 41]. This is consistent with the fact that most of the data analysed in ref. **31** were obtained from PSI of these organisms. On the other hand, the largest simulated lifetime of 9.6 μs, which dominates overall PhQ^- oxidation kinetics (Figure 2A), is more than 10 times slower than the longest-lived experimental lifetime, typically in the 200-350 ns range[1-5]. It is therefore not compatible with the experimental figures.

The presence of three components in the kinetics simulations with respect to the two most commonly encountered in the experiments, is due to the fact that three levels are included in the simulations (Figure 1, Eqn. 1). Nonetheless, when considering the "overall" phyllosemiquinone temporal evolution, given by $PhQ^{-}(t)$, it is also possible to calculate parameters such as the average $\tau_{av} = \sum_i A_i\tau_i / \sum_i A_i$ and the mean $\langle\tau\rangle = \int t \cdot PhQ^{-}(t)dt / \int PhQ^{-}(t)dt$ lifetime, that describe the population de-excitation in a fashion which is less dependent on the number of lifetimes considered.

For the simulation shown in Figure 2A, τ_{av} = 9.4 μs and $\langle\tau\rangle$ = 9.6 μs (Table 2). Both exceed by over 30 times the values of the same parameters estimated from the experimental results, which are in the 150< τ_{av} <280 ns and 235< $\langle\tau\rangle$ <350 ns ranges, respectively. Unsatisfactory descriptions of the experiments are also obtained for simulation considering values of –200 < $\Delta G^0_{F_X \to F_{A/B}}$ < –106 meV (Figure S1), 20 ≤ $\bar{\omega}_{F_x \to F_A}$ ≤ 550 cm^{-1} (Figure S2), and 0.5 < λ_i < 1 eV (Figure S3), which are presented in the Supplementary information. These are the only parameters for which a somewhat arbitrary (i.e. not taken from ref. **31**) value was adopted in the calculations of Figure 2A.

Thus, an energetic scenario involving a large uphill electron transfer between PhQ_A^- and F_X is unlikely, indicating that the value of $\Delta G^0_{PhQ_A \to F_X}$ is smaller than +125 meV. In this respect, the above discussed values of the slowest time constant and the overall PhQ^- oxidation kinetics are similar to those induced by the PsaA-F689N mutation in the PSI of *C. reinhardtii*[30], which was interpreted in terms of an up-shift of $E^0_{PhQ_A}$ of ~100-120 meV and those obtained in quinone substitution experiments[32-36] for redox moieties having comparable difference in their E^0 with respect to the naturally occurring PhQ.

Moreover this conclusion is supported also by the simulations performed using the calculated midpoint potential reported by Ishikita and Knapp[19], from which (+)119 < $\Delta G^0_{PhQ_A \to F_X}$ < 174 meV, considering that –705 < $E^0_{F_X}$ < –650 mV (Figure S4). For these energetic scenarios, the simulated kinetics of PhQ^- oxidation are

characterised by 6.4 $< \tau_{av} <$ 51 μs (Supplementary information), that are also not compatible with the experimental results.

It has been discussed that the number of crystallographic water molecules included in electrostatic calculations affects the estimate of the phylloquinones standard potential[20, 21]. The E^0 values shifted toward more electro-negative values by about 100 mV taking into account an extended water network[20] with respect to that considered initially in ref. **19**. Thereby, for the same interval for the F_X standard redox potential discussed above, it results that (+)21 $< \Delta G^0_{PhQ_A \rightarrow F_X} <$ 76 meV. Whereas the most positive values of $\Delta G^0_{PhQ_A \rightarrow F_X}$ are inconsistent with the experimental results (Figure S5), those which would put $\Delta G^0_{PhQ_A \rightarrow F_X} \cong k_B T$ (with T=290 K) reasonably approaches the experimental kinetics. On this basis, we suggest that $\Delta G^0_{PhQ_A \rightarrow F_X} \cong$ 30 mV is an upper boundary for this parameter, especially considering, as discussed in the proceeding, that value of λ_t = 0.7 eV represents a lower limit for the total reorganisation energy.

Since energetic models involving a large uphill energy transfer between PhQ_A^- and F_X is inconsistent with the experimental kinetics, we have then compared the other two scenarios discussed in the literature involving either i) "weak" driving forces coupled to PhQ_A^- oxidation, as initially proposed by Brettel[49] in the uni-directional electron transfer framework and successively extended to the bi-directional model[1] or ii) "large" driving forces, as derived from the values reported by Ptushenko *et al.*[21] from the electrostatic calculation accounting for non-isotropic values of the protein dielectric constant.

Large driving force coupled to PhQ_A^- *oxidation model.* Figure 2C shows the kinetic simulation obtained when the energetic scenario stemming from the values reported by Ptushenko and coworkers[21] is considered. The $E^0_{F_X}$ potential computed in ref. **21** is on the lower edge of experimentally determined distribution for this parameters[1-5, 12], resulting in $\Delta G^0_{F_X \rightarrow F_A}$ = –106 meV (Table 2). Hence, the simulation including the mean experimental value of $\Delta G^0_{F_X \rightarrow F_A}$ = –150 meV was also performed (Figure 2D). The latter value allows direct comparison with previous kinetic modelling[1, 22] and the other scenario investigated here. Identical values of λ_t = 0.7 eV

and couplings with mid-frequency nuclear modes characterised by $\bar{\omega}$ = 150 cm^{-1} were considered for all the reactions. Since this nuclear mode is relatively "soft", the high temperature approximation is valid at room temperature. Therefore these calculations are representative of any value of $\bar{\omega}$ < 150 cm^{-1}.

For these parameters, the PhQ^- oxidation kinetics is described by lifetimes of 0.7, 8.9 and 102 ns (Table 2) for $\Delta G^0_{F_X \to F_A}$ = –150 meV, and 0.7, 8.9 and 199 ns for $\Delta G^0_{F_X \to F_A}$ = –106 meV (Table 2), from which τ_{av} = 8.5 and 12 ns, respectively, and $\langle \tau \rangle$ = 53 and 127 ns, respectively. The simulated oxidations of PhQ^- are significantly faster than the experimental ones, for both the $\Delta G^0_{F_X \to F_A}$ considered. This is largely due to the two faster components (which have almost identical value for the two cases considered) that account for more than 90% of the overall PhQ^- population (Table 2). These lifetimes, particularly those in the range of ~10 ns, are compatible with values retrieved from experiments performed on cyanobacterial PS I [1-5, 12, 23]. This is noteworthy since the electrostatic calculations were based on the structural model of PSI purified from *Synechococcus. elongatus.* Thus, the scenario in which both PhQ_A^- and PhQ_B^- oxidation reactions are largely favourable, does not describe successfully the overall PhQ^- oxidation when λ_t = 0.7 eV. This might however stem from the particular value of λ_t adopted in the simulations of Figure 2C and 2D. This will be discussed further in the following, where simulations performed for different values of λ_t and $\bar{\omega}$ are presented.

Weak driving force coupled to PhQ_A^- *oxidation model.* Figure 2B shows the simulations performed considering the same set of parameters as in the calculations of Figure 2C, but with values of $\Delta G^0_{PhQ \to F_X}$ similar to those previously reported in the framework of weak driving forces coupled to PhQ^- oxidation[1, 5, 28-30], i.e. $\mp 2k_BT$. Since nuclear modes coupled to the electron transfer were not considered explicitly in previous kinetic modelling[1, 5, 28-30], an adjustment of the values of $\Delta G^0_{PhQ \to F_X}$ is introduced resulting in $\Delta G^0_{PhQ_A \to F_X}$ = +10 meV and $\Delta G^0_{PhQ_B \to F_X}$ = –50 meV (Table 1), which both fall in the interval of values previously deemed to be compatible with the

experimental observation[1]. We stress that the reported values for $\Delta G^0_{PhQ \rightarrow F_X}$ were not intended to accurate estimates, as their estimate depends on the choice of parameters set. The value of $\Delta G^0_{PhQ \rightarrow F_X}$ should have been considered as reasonable approximations and the same should hold true for the values reported in the present study.

The overall PhQ^- reduction kinetics is then described by lifetimes of 11, 22 and 289 ns (Table 2), yielding values of τ_{av} = 191 ns and $\langle\tau\rangle$ = 287 ns. These values closely resembles those determined experimentally, particularly those observed in PS I of green algae[1-5, 7, 8, 29, 30]. These simulations confirm that an energetic model considering asymmetric driving forces for F_X reduction, with the reaction involving PhQ^-_B thermodynamically favourable and the one involving PhQ^-_A being coupled to a shallow thermodynamic drive, is compatible with the experimental PhQ^- oxidation kinetics at room temperature.

The more satisfactory match to the experimental values for the "asymmetric weak driving force" with respect to the "asymmetric large driving force" model does not rule out the possibility that a scenario similar to that resulting from the computational studies by Ptushenko *et al.*[21] can appropriately describe the experimental observations, after appropriate choice of reorganisation energy and, to a lesser extent, of the mean nuclear mode frequency. The inclusion of a relatively weak nuclear mode $\bar{\omega}$ = 150 cm^{-1}, which is the only noticeable difference with respect to previous simulation studies[1] considering a "weak driving force" scenario, was not expected to change significantly the values of $\Delta G^0_{PhQ \rightarrow F_X}$ needed to simulate the kinetics at room temperature, as these were already chosen to yield a semi-quantitative description[1].

Dependency of the "weak driving force" and "large driving force" models for PhQ^- *oxidation by* F_X *on the value of the reorganisation energy* λ_t.

To explore the validity of the energetic models considered to be compatible with the experimental results and their robustness with respect to the chosen parameter sets, kinetic simulations were performed considering two different values

for the reorganisation energy: λ_t = 0.5 eV, or λ_t = 1 eV (see Experimental procedures).

When λ_t = 0.5 eV, with all the other parameters being the same as those used so far, the calculated PhQ^- oxidation kinetics are too rapid with respect to experimental results for both the energetic scenarios considered (Figure 3A and B). In both cases, the simulations deviate further from the experimental data with respect to those obtained for λ_t = 0.7 eV (Figure 2C, 2D). Considering a larger values of the nuclear mode, $\bar{\omega}$ >150 cm^{-1}, as suggested by molecular dynamics calculations[31], would lead to a further increase in the electron transfer rate and, thereby, in even faster lifetimes retrieved from kinetic modelling. Thus, it can be concluded that the reorganisation energy associated with both PhQ_A^- and PhQ_B^- oxidation is larger than 0.5 eV.

Increasing the value of λ_t from 0.7 to 1 eV, the energetic model suggested by Ptushenko and coworkers[21] resulted in a good description of the experimental results (Figure 3C). The PhQ^- decay shown in Figure 3C is characterised by lifetimes of 13 ns, 227 ns and 4.9 µs (Table 3). More than 90% of the PhQ^- is accounted by the two faster lifetimes, and the calculated τ_{av} = 294 ns is in a good agreement with the experiments. Instead the first moment of the decay distribution, $\langle\tau\rangle$ = 3.1 µs appears to exceed the experimental value. Yet, this is determined by the larger weight that the low amplitude 4.4 µs component has in the calculation of $\langle\tau\rangle$ with respect to τ_{av}. Hence, the slower electron transfer rates resulting from larger reorganisation energies provide a closer match to the experimental results for a model which involves large driving force for PhQ_A^- oxidation (i.e. $\Delta G^0_{PhQ_A \rightarrow F_X} < -50$ meV).

On the contrary, the kinetic description resulting from the "weak driving force" energetic scheme for λ_t = 1 eV (Figure 3D), are characterised by lifetimes of 211 ns, 426 ns and 5.1 µs. The corresponding values of τ_{av} = 3.1 µs and $\langle\tau\rangle$ = 5.1 µs exceed by a factor of ten those determined experimentally. This is a less satisfactory than that obtained for λ_t = 0.7 eV.

Hence, with an appropriate choice of λ_t, both energetic models are capable of describing the room temperature PhQ^- oxidation kinetics, even under the rather restrictive condition that $\lambda_{t,D\to A}$ assumes the same value for all the considered reactions. Whereas the assumption $\lambda_{t,PhQ_A\to F_X} \cong \lambda_{t,PhQ_B\to F_X}$ is reasonable due to the identical chemical nature of the cofactors involved and the overall similarity of the polarisable protein medium comprising the two phylloquinone binding niches, it is more likely that the value of $\lambda_{t,F_X\to F_{A/B}}$ is different and probably $\lambda_{t,F_X\to F_{A/B}} > \lambda_{t,PhQ\to F_X}$.

As the values of $\lambda_{t,PhQ\to F_X}$ and $\overline{\omega}_{PhQ\to F_X}$, as well as those of $\Delta G^0_{PhQ\to F_X}$, determine the temperature dependence of the rate constants (see Experimental procedures), it is informative to compare and test the two energetic schemes which describe satisfactorily the room temperature kinetics, with the experimental temperature dependence of PhQ^- oxidation.

Simulations of PhQ^- *oxidation temperature dependence.*

Whereas there is a large body of literature treating the room temperature kinetics of PhQ^- oxidation, studies of the reaction temperature dependence are far less abundant. This is particularly the case for the $PhQ_B^- \to F_X$ reaction which has been investigated only, to our knowledge, by Agalarov and Brettel[14], Santabarbara *et al.*[15] and Mula *et al.*[31]. In the first two studies the temperature range sampled was relatively limited, while a broader range was explored by Mula *et al.*[31]. A broad temperature range was also investigate by Schlodder *et al.*[13]. However, only the $PhQ_A^- \to F_X$ reaction was considered as the functionality of PhQ_B in electron transfer was not proven at that time. The experimental analysis of the temperature dependence of electron transfer reaction is, in most cases, reported in terms of lifetimes (or their inverse) as a function of the observation temperature, as these are the parameters which are directly accessible from fitting of kinetic traces. For instance, the parameters set used in the simulations of Figure 2A (and reported in Table 1) are taken from ref. **31**, in which the analysis was performed in terms of Equations 3-5, under the approximation $\tau = k_{et}^{-1}$. Yet, this approximation is valid only when the rate of forward electron transfer is much larger than that of the corresponding backward

reaction, i.e. when $\Delta G^0_{DA} \leq \sim -100$ meV. As discussed already, from the reported value of ΔG^*_{DA} and λ_t we obtain $\Delta G^0_{PhQ_A \rightarrow F_X}$ = +125 meV (Table 1). In this case, the $\tau = k_{et}^{-1}$ approximation ceases to be valid. For this reason the parameter set reported by Mula *et al.*[31] are inappropriate at describing the room temperature PhQ^- oxidation kinetics.

At the same time it should be noted that, whereas the outcome of kinetic modelling is also in terms of lifetimes (the ODE eigenvalues, see Experimental Procedures), their temperature dependence is determined by that of the individual electron transfer rate constants (the elements of the rate matrix, **K**). Each of these elements is described by Equations 3-5, that consider a single nuclear mode couple to each ET reaction. Although, this represents a simplified theoretical framework, it was shown to be rather solid (**e.g. 46, 47**). Moreover, considering several nuclear modes will lead to a steep increase in the number of adjustable parameters in the simulations, because, to our knowledge, these quantities have not been estimated either experimental or computationally.

Thus even considering these simplifications, the approach adopted here allows to compare the description of the *lifetimes* temperature dependence, which are the only parameters accessible experimentally, with the modelled lifetimes, which are the modelling outcome. Yet, the temperature dependences of the modelled lifetime stems from the actual *rate constants* temperature dependence, for which the theory applies more strictly. This represent, in our opinion, a significant improvement with respect to the standard analysis employed in previous studies.[†]

Definition of the acceptance confidence bounds of PhQ^- *oxidation temperature dependence.* For the reasons discussed above, the parameter sets reported by Mula *et al.*[31] can be considered as a realistic empirical description of the temperature dependence of the oxidation *lifetimes*, rather than the reaction rate constants. This macroscopic lifetime temperature dependence can then be used for a

[†] Since it is not expected that the uncertainties associated with each parameters are either all over- or under- estimated at the same time, these estimated confidence acceptance bound are, in all due respect, rather generous.

comparison with the kinetic simulation preformed at different temperatures (Figure 4 and 5). This defines what we will refer to hereafter as the "straight" extrapolation of the lifetime temperature dependence.

We notice that the computed lifetimes using the parameters from ref. **31** at 290 K are 9.5 and 361 ns for the fast and slow phases of PhQ^- oxidation, which fall in the lower and higher limits of the values reported in the experiments[1-5]. These values are close to the lifetimes most commonly reported for PS I isolated from cyanobacterial sources. Therefore, we have opted also to compare the simulations with extrapolations of temperature dependence, rescaled to yield values of 20 ns and 250 ns, at RT, respectively, which are instead closer to the values retrieved from the analysis of PS I from green algae[1-5]. This is equivalent to vary only the value of $|H_{DA}|^2$ and defines what we will refer to hereafter as the "rescaled" extrapolation of the lifetime temperature dependence. We consider that this would yield a more general breath to the simulation results, since species-specific differences in the details of the parameters controlling this ET reaction might exist[43, 44].

Finally, there is a margin of uncertainties associated with the reported parameters and it is reasonable to assume that the confidence level is, at least, about 5%, that of the best-fit values. Thereby upper and lower boundaries defining an "acceptable" range towards which the simulation are tested were also computed (dashed lines in Figure 4 and 5). These estimated uncertainty bounds define the acceptance spread within which the simulated lifetime temperature dependences are expected to fall[§].

Large driving force model. In Figure 4A the temperature dependence of the three lifetimes resulting from kinetic simulations performed utilizing the same parameters as in Figure 3C (i.e. λ_i = 1 eV and $\bar{\omega}$ = 150 cm^{-1}) for the large (asymmetric) driving forces (Table 1) are compared with the experimental extrapolation. The same results are also presented in Figure 4B as the Arrhenius plot.

The simulations performed at 290 K (Figures 2C, D and 3A, C) indicate that PhQ^- oxidation is described almost exclusively by the two faster lifetimes (τ_1 and τ_2), whereas the slowest one (τ_3) is primarily associated to the oxidation of F_X. Hence it is the value of the two faster lifetime which should be compared with the

values extrapolated from the experiments. The temperature dependence of the fastest lifetime τ_1 (Figure 4A, open circles) is close to the extrapolated upper acceptance limit, and slightly outside it for $T <$ 220 K. Moreover, the simulated apparent activation (we use apparent as the actual activation is that associated with the rate constants, and which is presented in Figure S6 of the Supplementary Information**,** rather than the lifetimes) is larger than that extrapolated from the experiments. Still, the larger deviations occur at temperature where the fast phase of PhQ^- was not experimentally detectable. On the other hand, the temperature dependence of τ_2 (Figure 4A, open squares) falls on the lower limit of the estimated acceptance spread. The apparent lifetime activation behaviour is well reproduced by the kinetic simulations.

Figure 4C (and D for the Arrhenius plot) shows the comparison between the simulated lifetimes and the "rescaled" experimental temperature dependence. In this case, both the simulated τ_1 and τ_2 lifetimes temperature dependences fall in the range compatible with the experimental results. This congruency is particularly relevant taking into account both the modelling approximations and the uncertainties associated to the experimental values.

The most obvious deviation from the experimental extrapolation is the steeper apparent activation of the fast oxidation PhQ^- phase (τ_1) in the simulation. The temperature dependent profile is determined by the parameters in the Frank-Condon factors that, besides the standard free and reorganisation energies, involves also the mean nuclear mode coupled to the electron transfer reactions. Molecular dynamics computation[31] indicated that $\bar{\omega}_{PhQ_B \to F_X}$ is about two times larger than $\bar{\omega}_{PhQ_A \to F_X}$ (Table 1), because of differences in hydrogen bonding to the two phylloquinones present in PS I. Therefore, kinetic simulations for the large driving force model were performed also considering $\bar{\omega}_{PhQ_B \to F_X}$ = 378 cm^{-1} and $\bar{\omega}_{PhQ_A \to F_X}$ = 173 cm^{-1}. For the value of $\bar{\omega}_{F_X \to F_A}$ which was not reported, we used, as above, an intermediate value of 275 cm^{-1}. These simulations yield a closer agreement between the then modelled fastest lifetime (τ_1) and the experimental extrapolation of its temperature dependence (Figure 4A, solid circles); τ_1 becomes faster and less dependent on temperature, as expected for a relatively large value of $\bar{\omega}$. Yet, whereas the simulated τ_1 temperature

dependence fell within the confidence band derived from the parameter of ref. **31** (Figure 4A), the comparison with the "rescaled" expectancy bounds (Figure 4C) suggest that τ_1 is slightly underestimated. Instead, the temperature dependence of τ_2 is much less affected when considering $\bar{\omega}_{PhQ_A \rightarrow F_X}$ = 173 cm^{-1}. This is because the latter value does not differ significantly from the 150 cm^{-1} (for all the ET reactions) used so far. It falls slightly outside the lower edge of the confidence limits obtained using the parameters straight from the study of Mula *et al.*[31], whereas it is on the lower boundary limit of the acceptable range after "rescaling", indicating that the reaction rate constant is overestimated, irrespectively to the system to which it is compared. Thus, in this simulation both lifetimes, τ_1 and τ_2, are on the lower edge of the acceptance spread, with τ_2 being slightly outside it, but, on the other hand, the apparent temperature dependence is quite nicely reproduced. Moreover, irrespectively of the value of $\bar{\omega}_{F_X \rightarrow F_A}$ considered, τ_3, that primarily described the oxidation of F_X^-, is the slowest process in this energetic scenario at all the temperature considered.

Weak driving force model. The comparison between the lifetime temperature dependence obtained for the weak driving simulations and the extrapolation of the experimental lifetimes is shown in Figure 5, also as the Arrhenius plot. Values of λ_t = 0.7eV and a mean nuclear mode of $\bar{\omega}$ = 150 cm^{-1} were considered, as in simulations of Figure 2B. For this energetic scenario, PhQ^- oxidation is described primarily by the fastest and slowest lifetimes τ_1 and τ_3, whereas τ_2 has small amplitude (Table 2). At odds with the large driving force model, it is not possible to assign a specific lifetime to the oxidation of F_X^- which decay is overlapped temporally to that of PhQ_A^- (Figure 2B). Thus, it is the temperature dependence of τ_1 and τ_3 that should be compared with the acceptance spread of extrapolated experimental values. The *rate constants* temperature dependence for this model is presented in Figure **S6** of the Supplementary Information instead**.**

When assuming $\bar{\omega}$ = 150 cm^{-1} for all reactions, τ_1 falls within the confidence limit at temperature higher than 250 K, but exceeds the upper bounds at lower temperatures (Figure 5A, open circles). A less significant deviation is observed when considering the "scaled" experimental extrapolation (Figure 5C). This is consistent

with the simulations preformed at RT for the same energetic scenario which resulted in a description more close to the experimental value retrieved in PSI of green algae rather than of cyanobacteria. However, even in this case, the apparent activation is larger than the experimental extrapolation. The value of τ_3 is also within the confidence bounds for temperature higher than 250 K, but tends to deviate from the extrapolated acceptance spread at lower temperatures, where the simulation predicts more rapid kinetics than the experimental values. In general, for this energetic model, τ_3 shows a smaller apparent activation than that observed for the τ_2 resulting from the large driving force model, and with respect to the extrapolation of the experimental results.

Simulations considering nuclear modes of frequencies $\bar{\omega}_{PhQ_B \rightarrow F_X}$ = 378 cm^{-1} and $\bar{\omega}_{PhQ_A \rightarrow F_X}$ = 173 cm^{-1} and an intermediate value for $\bar{\omega}_{F_X \rightarrow F_A}$ = 275 cm^{-1} were also performed for the weak driving force energetic scenario (Figure 5A, solid symbols). A decrease in the values of τ_1 and a closer agreement with the experimental extrapolation is obtained, although on the lower edge of the acceptance interval (Figure 5A, solid circles). The apparent τ_1 activation was damped and it becomes only slightly smaller than that predicted from the experiments extrapolations. The value of τ_3 also became faster, as expected from increasing the values of the electron transfer rates. Similar to the simulations performed for an homogeneous value of $\bar{\omega}$ = 150 cm^{-1}, the values of the slowest lifetime, τ_3, fell within the range that we consider compatible with the experimental results, at least above 250 K, especially when compared to the rescaled experimental extrapolation (Figure 5C), but some deviations occur at lower temperatures. Hence, the activation of the slow phase of PhQ^- is described less precisely by the weak driving force compared to the large driving force model. Since these calculations do not involve any attempt at the optimisation of the parameters, both these energetic models can be considered compatible with the experimental results.

To a semi-quantitative level some general conclusions can be drawn:

i) It is likely that a mean nuclear mode of mid-high frequency, i.e. close to 378 cm^{-1}, the value predicted by the molecular dynamics, is coupled to the $PhQ_B^- \rightarrow F_X$ reaction. Considering a lower frequency mode, for

values of $-259 < \Delta G^{0}_{PhQ_B \rightarrow F_X} < -50$ meV and values of $0.7 < \lambda_t < 1$ eV, resulted in too large activations of the fast phase. Such deviation was amended once the mid-high frequency mode was considered. On the other hand, this led to value of the lifetimes associated with the fast phase of PhQ^- which were on the lower limit of the experimental spread.

ii) The value of the total reorganisation energy $\lambda_t = 0.7$ eV is likely a lower bound. In fact, the temperature dependence of τ_3, obtained for the shallow equilibrium model which considered such figure, appeared weaker than those extrapolated from the experiments, indicating that λ_t might be underestimated.

iii) The predictions of a mid-soft mode of ~170 cm^{-1} coupled to $PhQ_A^- \rightarrow F_X$ represents an higher bound for this parameter. Independently of the other values considered, the simulated values of the slower PhQ^- lifetime tend slightly toward the upper limit of reported values (i.e. 200 ns, compared to the experimental values of 250-350 ns) and the apparent activation is, if anything, less pronounced than in the experimental extrapolations.

Comparison of the "weak" and "large" driving force models at room temperature when considering unequal values of $\overline{\omega}_{PhQ \rightarrow F_X}$.

In this conclusive session, the description of PhQ^- oxidation and F_X oxidation-reduction kinetics at room temperature, in the framework of semi-optimised "weak" and "large" driving-forces models, will be discussed. For semi-optimised we intend using the same set of parameters which yield the closer agreement to the experimental data for each model (as in Figure 1-4 and tables 1-3), but including asymmetric values of $\overline{\omega}_{PhQ \rightarrow F_X}$ [31], as this was shown to improve the description of the lifetime temperature dependence (Figures 4 and 5).

The time evolutions obtained by the simulations are presented in Figure 6. For the weak driving force model the predicted lifetimes are 5.1, 18 and 220 ns, yielding an average lifetime τ_{av} = 144 ns and $\langle \tau \rangle$ = 220 ns. For the large driving force

scenario the kinetic simulations yield lifetimes of 4.7, 152 ns and 2.0 µs, yielding an average lifetime τ_{av} = 151 ns and $\langle\tau\rangle$ = 1.1 µs.

Although for both energetic scenarios the simulated lifetimes are close to the lower limit of the spread reported for experimental values, they can be considered to be in fair semi-quantitative agreement. A closer match between simulation and experimental results could be obtained by an appropriate choice of the parameters describing the ET rates. Yet, this would involve the optimisation of too many microscopic parameters that have not been directly or indirectly assessed either experimentally or computationally. Therefore, we consider a semi-quantitative description and discussion more appropriate. Even on such semi-quantitative basis, differences in the simulated ET kinetics based on the two energetic models considered in this section, are apparent:

i) in the large driving force model, the oxidation of PhQ_A^- and PhQ_B^- are relatively separated in time (Figure 6B), each being dominated by one of the retrieved lifetimes. For the weak driving force model (Figure 6A) the oxidation of both phyllo(semi) quinone is biphasic, even though each is dominated by either the fastest (PhQ_B^-) or slowest (PhQ_A^-) lifetimes. This makes the temporal evolution of the two species more overlapped in time with respect to the large driving force model.

ii) In the large driving force model, the relative amplitude associated to each kinetic phase is essentially determined by the initial population of PhQ_A^- and PhQ_B^-, that has been assumed to be equal in these calculations (Figure 6B). On the other hand, for the weak driving force model, the relative amplitude of the two phases differs from the initial population (Figure 6A). The slow phase increases in amplitude as a result of a net population transfer from PhQ_B^- to PhQ_A^-, mediated by F_X, which has previously been discussed[5, 29,30].

iii) In the large driving force model, the slowest lifetime and, as a result, the slowest decaying species is the one associated with the F_X cofactor, which is predicted to be reduced with an average time of

78 ns and oxidised with a mean time of 2.0 μs (Figure 6B). On the other hand, for the weak driving force model, the oxidation of PhQ_A^- and that of F_X^- overlaps, as the latter is predicted to be populated in 5 ns and decay with an average lifetime of 140 ns (Figure 6A).

Experimental determination of the lifetime characterising the $F_X^- \rightarrow F_{A/B}$ electron transfer reaction are not abundant. This is because its detection is technically challenging, due to the weak extinction coefficient and the broad and relatively unstructured band-shape of the absorption spectrum of these cofactors, that have the same chemical nature. Nonetheless, most experimental evidences indicate that this ET reaction takes place in 100-300 ns [1, 6, 12, 23, 50-54], which is closer to the estimate obtained for the weak driving force model. However, there has been no attempt here at optimising the ET reactions involving F_X for the large driving force model: the simulation results from parameter sets which best describe the PhQ^- oxidation kinetics. Taken this into account this discrepancy does not represent a sufficient argument to discard the large driving force energetic scenario when concerning the PhQ^- oxidation reactions. Yet, for $F_X^- \rightarrow F_{A/B}$ to become significantly faster, as observed in the experiment, the energetic model would require either a much larger value of $\overline{\omega}_{F_X \rightarrow F_{A/B}}$ and/or $\Delta G^0_{F_X \rightarrow F_{A/B}}$ (the latter was taken from ref. **21**), or a significantly smaller value of λ_i, which appears less likely by virtue that this ET reactions involves metal centres.

Conclusions

In this study we have tested different energetic models and set of parameters describing the electron transfer rates associated with the PhQ^- oxidation reactions by F_X in PS I. From our modelling analysis we conclude that two energetic models, one considering asymmetric low driving forces for PhQ_A^- ($\Delta G^0_{PhQ_A \rightarrow F_X} \cong$ 10 meV) and PhQ_B^- ($\Delta G^0_{PhQ_B \rightarrow F_X} \cong$ –50 meV) oxidation[1], the other considering larger driving forces for PhQ_A^- ($\Delta G^0_{PhQ_A \rightarrow F_X} \cong$ –100 meV) and PhQ_B^- ($\Delta G^0_{PhQ_A \rightarrow F_X} \cong$ –250 meV) oxidation[21], are compatible with the experimental kinetics at 290 K, assuming values of the total

reorganisation energy, λ_r, equal to 0.7 and 1 eV, respectively. Both energetic models were also shown to be consistent with the temperature dependence of the PhQ^- oxidation lifetime extrapolated from the experiments.

This analysis indicates that more in-depth experimental characterisation of the PhQ^- oxidation kinetics is still necessary to uncover the molecular properties underpinning this crucial electron transfer step in the PS I electron transfer chain. Understanding of the energetic properties associated with these ET transfer reactions is significant because it has been proven that PSI shows remarkable plasticity to alterations of the PhQ binding site[1-5]: the overall PhQ^- oxidation rate *e.g.* [1-5, 8, 28, 31, 51, 52] and fractional utilisation of the two functional cofactor chains *e.g.* [1-5, 30, 40-43. 51, 52] can be modulated by single amino acid substitutions without significant losses in the reaction centre quantum yield[30,52]. These aspects are therefore important under evolutionary point of view, since this plasticity allows for changes in the functionality of the system when maintain its functional robustness[30], and under biotechnological perspective, since PSI appears to be particularly suited to be engineered for tailored applications, particularly to hybrid photovoltaics *e.g.* [55-57]. To this end a better understanding of the factors controlling the reactions is required. It is to be foreseen that a detailed investigation of the temperature dependence of mutants which affects PhQ^- oxidation over a sufficiently broad temperature range, in combination with refined kinetic modelling of the kind presented here and quantum chemical/electrostatic calculations, as performed in previous studies, would be beneficial and might lead to a throughout comprehension of these processes.

Acknowledgements. We thank Dr. A.P. Casazza (IBBA, CNR, Milan, Italy) for fruitful comments and suggestions on the redaction of this manuscript.

Electronic Supplementary Information (ESI) available: Kinetic modelling for different parameter sets, in the framework of the large energetically uphill PhQ_A^- oxidation by F_X, are performed and the outcome discussed; temperature dependence of the electron transfer rate constants.

References

1. S. Santabarbara, P. Heathcote and M.C.W. Evans, *Biochim. Biophys. Acta – Bioenergetics,* 2005, **1708**, 283–310.

2. F. Rappaport, B.A. Diner and K.E. Redding, in *Photosystem I: The Light–Driven Plastocyanin:Ferredoxin Oxidoreductase*, ed. J.H. Golbeck, Kluwer Academic Publishers, Dordrecht, 2006, pp. 223-244.

3. N. Srinivasan and J.H. Golbeck, *Biochim. Biophys. Acta – Bioenergetics*, 2009, **1787**, 1057–1088.

4. K.E. Redding and A. van der Est, in *Photosystem I: The Plastocyanin:Ferredoxin Oxidoreductase in Photosynthesis*, ed. J.H. Golbeck, Kluwer Academic Publishers, Dordrecht, 2006, pp. 413–437

5. S. Santabarbara, L. Galuppini, and A. P. Casazza, *J. Integr. Plant. Biol.,* 2010, **52**, 735-749.

6. P. Joliot and A. Joliot, *Biochemistry*, 1999*,* **38***,* 11130-11136.

7. I.P. Muhiuddin, P. Heathcote, S. Carter, S. Purton, S.E. Rigby, and M.C.W. Evans, *FEBS Lett.*, 2001, **503**, 56-60.

8. M. Guergova–Kuras, B. Boudreaux, A. Joliot, P. Joliot and K.E. Redding, *Proc. Natl. Acad. Sci. USA*, 2001, **98**, 4437–4442.

9. S. Santabarbara, I. Kuprov, W.V. Fairclough, S. Purton, P.J. Hore, P. Heathcote and M.C.W. Evans, *Biochemistry*, 2005, **44**, 2119–2128.

10. O.G. Poluektov, S.V. Paschenko, L.M. Utschig, K.V. Lakshmi, and M.C. Thurnauer, *J. Am. Chem. Soc.*, 2005, **127**, 11910-11911.

11. W. Giera, K. Gibasiewicz, V.M. Ramesh, S. Lin and A. Webber, *Phys. Chem. Chem. Phys.*, 2009, **11**, 5186–5191.

12. K. Brettel, *Biochim. Biophys. Acta – Bioenergetics*, 1997*,* **1318***,* 322–373.

13. E. Schlodder, K. Falkenberg, M. Gergeleit, and K. Brettel, *Biochemistry*, 1998, **37**, 9466–9476.

14. R. Agalarov and K. Brettel, *Biochim. Biophys. Acta – Bioenergetics*, 2003, **1604**, 7–12.

15. S. Santabarbara, K.E. Redding and F. Rappaport, *Biochemistry*, 2009, **48**, 10457–10466.

16. P. Jordan, P. Fromme, H.T. Witt, O. Klukas, W. Saenger and N. Krauss, *Nature*, 2001, **411**, 909–917.

17. A. Ben–Shem, F. Frolow and N. Nelson, *Nature*, 2003, **426**, 630–635

18. T. Berthold, E.D. von Gromoff, S. Santabarbara, P. Stehle, G. Link, O.G. Poluektov, P. Heathcote, C.F. Beck, M.C. Thurnauer and G. Kothe, G., *J. Am. Chem. Soc.*, 2012, **134**, 5563–5576.

19. H. Ishikita and Knapp, *J. Biol. Chem.*, 2003, **278**, 52002–52011.

20. I. Karyagina, Y. Pushkar, D. Stehlik, A. van der Est, H. Ishikita, E.W. Knapp, B. Jagannathan, R. Agalarov and J.H. Golbeck, *Biochemistry*, 2007, **46**, 10804-10816.

21. V.V. Ptushenko, D.A. Cherepanov, L.I. Krishtalik and A.Y. Semenov, *Photosynth Res.*, 2008, **97**, 55 –74.

22. C.C. Moser and P .L.Dutton, P.L. in *Photosystem I: The Light–Driven Plastocyanin:Ferredoxin Oxidoreductase*, ed. J.H. Golbeck, Kluwer Academic Publishers, Dordrecht, 2006, pp. 583-594.

23. K. Brettel and W. Leibl, *Biochim. Biophys. Acta*, 2001, **1507**, 100–114.

24. S.K. Chamorowsky and R. Cammack, *Photochem. Photobiophys.*, 1982, **4**, 195–200.

25. B. Ke, W.A. Bulen, E.R. Shaw and R.H. Breeze, *Arch. Biochem. Biophys.*, 1974, *162*, 301–309.

26. B. Munge, S.K. Das, R. Ilagan, Z. Pendon, J. Yang, H.A. Frank and J.F. Rusling, *J. Am. Chem. Soc.*, 2003, **125**, 12457–12463.

27. M. Iwaki, S. Kumazaki, K. Yoshihara, T. Erabi and S. Itoh, *J. Phys. Chem.*, 1996, **100**, 10802–10809.

28. K. Ali, S. Santabarbara, P. Heathcote, M.C.W. Evans and S. Purton, *Biochim. Biophys. Acta – Bioenergetics*, 2006, **1757**, 1623–1633.

29. S. Santabarbara, K. Reifschneider, A. Jasaitis, F. Gu, G. Agostini, D. Carbonera, F. Rappaport and K.E. Redding, *J. Phys. Chem. B.*, 2010, **114**, 9300–9312.

30. S. Santabarbara, B. Bullock, F. Rappaport and K.E. Redding, *Biophys. J.*, 2015, **108**, 1537– 1547.

31. S. Mula, M.D. McConnell, A. Ching, N. Zhao, H.L. Gordon, G. Hastings, K.E. Redding and A. van der Est, *J. Phys. Chem. B.*, 2012, **116**, 14008-14016.

32. S. Mula, A. Savitsky, K. Mobius, W. Lubitz, J.H. Golbeck, M.D. Mamedov, A.Y. Semenov and A. van der Est, *Photochem. Photobiol. Sci*., 2012, **11**, 946–956.

33. H. Makita, N. Zhao and G. Hastings,. *Biochim. Biophys. Acta*, 2015, **1847**, 343–354.

34. T.W. Johnson, G. Shen, B. Zybailov, D. Kolling, R. Reategui, S. Beauparlant, I.R. Vassiliev, D.A. Bryant, A.D. Jones, J.H. Golbeck and P.R. Chitnis, *J. Biol. Chem.*, 2000, **275**, 8523–8530.

35. A.Y. Semenov, I.R. Vassiliev, A. van Der Est, M.D. Mamedov, B. Zybailov, G. Shen, D. Stehlik, B.A. Diner, P.R. Chitnis and J.H. Golbeck, *J. Biol. Chem.*, 2000, **275**, 23429–23438.

36. K.M. Bandaranayake, R. Wang, T.W. Johnson and G. Hastings, *Biochemistry*, 2006, **45**, 12733–12740.

37. R.A. Marcus and N. Sutin, *Biochim. Biophys. Acta*, 1985, **811**, 265–322.

38. D. Devault, *Quantum mechanical tunnelling in biological systems*, Cambridge University Press, Cambridge, 1980.

39. J.J. Hopfield, *Proc. Natl. Acad. Sci. USA*, 1974, **71**, 3640–3644.

40. W. Xu, P. Chitnis, A. Valieva, A. van der Est, Y.N. Pushkar, M. Krzystyniak, C. Teutloff, S.G. Zech, R. Bittl, D. Stehlik, B. Zybailov, G. Shen and J.H. Golbeck, *J. Biol. Chem.*, 2003, **278**, 27876– 27887.

41. R.O. Cohen, G. Shen, J.H. Golbeck, W. Xu, P.R. Chitnis, A.I. Valieva, A. van der Est, Y. Pushkar and D. Stehlik, *Biochemistry*, 2004, **43**, 4741–4754

42. S. Santabarbara, I. Kuprov, P.J. Hore, A. Casal, A., P. Heathcote and M.C.W. Evans, *Biochemistry*, 2006, **45**, 7389 –7403.

43. S. Santabarbara, I. Kuprov, O.G. Poluektov, A. Casal, C.A. Russell, S. Purton and M.C.W. Evans, *J. Phys. Chem. B.*, 2010, **114**, 15158–15171.

44. M.D. McConnell, J. Sun, R. Siavashi, A. Webber, K.E. Redding, J.H. Golbeck and A. van der Est, *Biochim Biophys Acta – Bioenergetics*, 2015, **1847**, 429– 40.

45. M.H. Vos and H.J. van Gorkom, *Biophys. J.*,1990, **58**, 1547–1555.

46. C.C. Moser and P.L. Dutton, *Biochim. Biophys. Acta*, 1992, **1101**, 171–176.

47. C.C. Page, C.C. Moser, X. Chen and P.L. Dutton, *Nature*, 1999, **402**, 47–52.

48. V.M. Ramesh, M. Guergova-Kuras, P. Joliot and A.N. Webber, *Biochemistry*, 2002, **41**, 14652–14658.

49. K. Brettel, in *Photosynthesis: mechanism and Effect*, ed. G. Garab, Kluwer Academic Publisher, Dordrech, 1998, pp. 611–614.

50. J. Lüneberg, P. Fromme, P. Jekow and E. Schlodder, *FEBS Lett.*, 1994, **338**, 197–202

51. M. Byrdin, S. Santabarbara, F., Gu, V.W. Fairclough, P. Heathcote, K.E. Redding and F. Rappaport, *Biochim. Biophys. Acta – Bioenergetics*, 2006, **1757**, 1529–1538.

52. S. Santabarbara, A. Jasaitis, M. Byrdin, F. Gu, F. Rappaport and K.E. Redding, *Photochem. Photobiol.*, 2008, **84**, 1381–1387.

53. W. Leibl, B. Toupance and J. Breton, *Biochemistry*, 1995, **34**, 10237–10244.

54. P- Setif and K. Brettel, *Biochemistry*, 1993, **32**, 7846–7854.

55. C.E. Lubner, P. Knörzer, P.J. Silva, K.A. Vincent, T. Happe, D.A. Bryant, and J.H. Golbeck, *Biochemistry*, 2010, **49**, 10264–10266.

56. S.C. Silver, J. Niklas, P. Du, O.G. Poluektov, D.M. Tiede, and L.M. Utschig, *J. Am. Chem. Soc.* 2013, **135**, 13246–13249.

57. D. Gunther, G. LeBlanc, D. Prasai, J.R. Zhang, D.E. Cliffel, K.I. Bolotin, and G.K. Jennings, *Langmuir*, 2013, **29**, 4177–4180.

Table 1. ***Parameters controlling the electron transfer rates associated with*** PhQ^- ***and*** F_X ***oxidation/reduction according to different energetic model scenarios.***

Reaction	ΔG^0 (eV 10^{-3})	$\lvert H_{DA}\rvert^2$ (eV^2 10^{-6})	$\bar{\omega}$ (cm^{-1})	k_{et}^{-1} (ns^{-1})	ΔG^* (eV 10^{-3})
Large uphill PhQ_A^- *oxidation* [a]					
$PhQ_A^- \rightarrow F_X$	125	1.04	173	361	243
$PhQ_B^- \rightarrow F_X$	-58	0.54	378	9.5	147
$F_X^- \rightarrow F_{A/B}$	-150	0.028	275	73	108
Large driving force for PhQ_A^- *oxidation* [c]					
$PhQ_A^- \rightarrow F_X$	-86	0.81	150	9.27	135
$PhQ_B^- \rightarrow F_X$	-259	0.95	150	0.70	69
$F_X^- \rightarrow F_{A/B}$	-106	0.028	150	192	126
Weak driving force for PhQ_A^- *oxidation* [b]					
$PhQ_A^- \rightarrow F_X$	10	0.81	150	50	180
$PhQ_B^- \rightarrow F_X$	-50	0.95	150	14	150
$F_X^- \rightarrow F_{A/B}$	-150	0.028	150	98	108

Compilation of parameter sets associated with oxidation/reduction of $PhQ_{A/B}$ and F_X, used in kinetic modelling for different energetic scenarios, which are shown in Figure 2. The simulations outcome in terms of amplitudes and lifetimes is presented in Table 2. The values of $\Delta G^0_{PhQ_{A/B}^- \rightarrow F_X}$ are taken from ref. **31** (a), this study (b), ref. **21** (c). The (total) reorganisation energy λ_t was 0.7 eV in all cases.

Table 2. ***Parameters describing the*** PhQ^- ***oxidation kinetics resulting from simulations considering different energetic scenarios.***

Large uphill PhQ_A^- *oxidation* [a]					
	Lifetime (ns)	$A_{PhQ_A^-}$	$A_{PhQ_B^-}$	$A_{F_X^-}$	$A_{PhQ_{tot}^-}$
τ_1	2.6	0.17	0.007	-0.19	0.18
τ_2	9.9	-0.65	0.49	0.18	-0.16
τ_3	9612	0.97	0.0007	0.007	0.97
τ_{av} (ns)	$\langle\tau\rangle$ (ns)				$A_{PhQ^-}^{fast} : A_{PhQ^-}^{slow}$
9366	9613				0.03:0.97
Weak driving force for PhQ_A^- *oxidation* [b]					
	Lifetime (ns)	$A_{PhQ_A^-}$	$A_{PhQ_B^-}$	$A_{F_X^r}$	$A_{PhQ_{tot}^-}$
τ_1	11	0.28	0.31	-0.67	0.59
τ_2	22	-0.39	0.13	0.33	-0.26
τ_3	289	0.61	0.052	0.34	0.66
τ_{av} (ns)	$\langle\tau\rangle$ (ns)				$A_{PhQ^-}^{fast} : A_{PhQ^-}^{slow}$
191	287				0.34:0.66
Large driving force for PhQ_A^- *oxidation* [c]					
$\Delta G^0_{F_X \to F_{A/B}} = -106$ meV					
	Lifetime (ns)	$A_{PhQ_A^-}$	$A_{PhQ_B^-}$	$A_{F_X^r}$	$A_{PhQ_{tot}^-}$
τ_1	0.70	0.001	0.50	-0.50	0.50
τ_2	8.9	0.46	-2E-05	-0.48	0.46
τ_3	199	0.04	4E-05	0.99	0.04
τ_{av} (ns)	$\langle\tau\rangle$ (ns)				$A_{PhQ^-}^{fast} : A_{PhQ^-}^{slow}$ *
11.9	127				0.96:0.04
$\Delta G^0_{F_X \to F_{A/B}} = -150$ meV					
	Lifetime (ns)	$A_{PhQ_A^-}$	$A_{PhQ_B^-}$	$A_{F_X^r}$	$A_{PhQ_{tot}^-}$
τ_1	0.70	0.001	0.5	-0.50	0.50
τ_2	8.9	0.46	-2 E-05	-0.50	0.46
τ_3	102	0.04	4 E-05	1	0.04
τ_{av} (ns)	$\langle\tau\rangle$ (ns)				$A_{PhQ^-}^{fast} : A_{PhQ^-}^{slow}$ *
8.5	53				0.90:0.04

Amplitude (A_i) and lifetimes (τ_i) describing the oxidation/reduction kinetics of with $PhQ_{A/B}$ and F_X resulting from different energetic models, presented in Figure 2. The models input parameters are listed in Table 1 and taken from ref. **31** (a), this study (b), ref. **21** (c). $A_{PhQ^-_{tot}} = A_{PhQ^-_A} + A_{PhQ^-_B}$, τ_{av} is the average lifetime ($\sum_i A_i\tau_i / \sum_i A_i$), $\langle\tau\rangle$ is the mean lifetime ($\int t \cdot f(t)dt / \int f(t)dt$) and $A^{fast}_{PhQ^-} : A^{slow}_{PhQ^-}$ is the normalised fractional amplitude of fast and slow PhQ^- oxidation phases, with $A^{slow}_{PhQ^-}$ being the sum the PhQ^-_{tot} amplitudes associated with $\tau_i > 80$ ns.

Table 3. ***Parameters describing the*** PhQ^- ***oxidation kinetics resulting from simulations considering different reorganisation energies.***

Large driving force for PhQ_A^- *oxidation* [a]

	λ_t =0.5 eV					λ_t =1 eV				
	Lifetime (ns)	$A_{PhQ_A^-}$	$A_{PhQ_B^-}$	$A_{F_X^-}$	$A_{PhQ_{tot}^-}$	Lifetime (ns)	$A_{PhQ_A^-}$	$A_{PhQ_B^-}$	$A_{F_X^-}$	$A_{PhQ_{tot}^-}$
τ_1	0.14	0.002	0.50	-0.50	0.50	12.6	0.001	0.50	-0.50	0.50
τ_2	1.4	0.46	-2E-05	-0.48	0.46	227	0.46	-2E-05	-0.48	0.46
τ_3	31	0.04	4.E-05	0.99	0.04	4916	0.037	4E-05	0.99	0.04
	τ_{av} (ns)				$A_{PhQ^-}^{fast} : A_{PhQ^-}^{slow}$	τ_{av} (ns)				$A_{PhQ^-}^{fast} : A_{PhQ^-}^{slow}$
	1.9				0.50:0.50	294				0.50:0.50

Weak driving force for PhQ_A^- *oxidation* [b]

	λ_t =0.5 eV					λ_t =1 eV				
	Lifetime (ns)	$A_{PhQ_A^-}$	$A_{PhQ_B^-}$	$A_{F_X^-}$	$A_{PhQ_{tot}^-}$	Lifetime (ns)	$A_{PhQ_A^-}$	$A_{PhQ_B^-}$	$A_{F_X^-}$	$A_{PhQ_{tot}^-}$
τ_1	1.5	0.28	0.32	-0.67	0.59	211	0.28	0.31	-0.67	0.59
τ_2	3.0	-0.39	0.13	0.32	-0.25	426	-0.39	0.14	0.33	-0.25
τ_3	42.5	0.60	0.05	0.35	0.66	5154	0.618	0.051	0.34	0.66
	τ_{av} (ns)				$A_{PhQ^-}^{fast} : A_{PhQ^-}^{slow}$	τ_{av} (ns)				$A_{PhQ^-}^{fast} : A_{PhQ^-}^{slow}$
	28.0				0.34:0.66	3431.69				0.34:0.66

Amplitude (A_i) and lifetimes (τ_i) describing the oxidation/reduction kinetics of with $PhQ_{A/B}$ and F_X resulting from the "large" (*a*: ref. 21) and "weak" (*b*: this study) driving force models, for different values of λ_t . The simulated kinetics are shown in Figure 3. All other model input parameters are listed in Table 1. All symbols are in the legend of Table 2.

Figure Legends.

Figure 1. A: Schematic representation of the cofactors involved in secondary electron transfer reactions in Photosystem I. PhQ_A (red), PhQ_B (blue), F_X (gold) and $F_{A/B}$ (yellow). Also shown is the reaction scheme considered in kinetic simulations, as in the ordinary differential equation system of Eqn. 1 . **B**: Schematic representation of the spread of standard redox potential for PhQ_A^- / PhQ_A with respect to F_X^r / F_X . The dashed box indicate energetic scenarios in which the reaction can be considered as largely uphill (red), coupled to a weak driving force (orange) or coupled to a large driving force (violet). The red tick line are values from ref. **31,** and the violet think line from ref. **21**. Orange think lines highlights the interval of more likely values suggested in ref. **1**.

Figure 2. Simulations of PhQ^- oxidation kinetics at room temperature (T= 290 K) for different energetic configuration of the redox cofactors involved in secondary electron transfer reactions in PSI. **A**: "large uphill electron transfer" using the parameters reported by Mula *et al.* (**31**) and listed Table 1. **B:** "weak-driving-force" scenario, modified from Santabarara *et al.* (**1**) and Table 1. **C:** "large-driving-force" model, using the parameters reported by Ptushenko *et al.* (**21**) and Table 1; **D:** "large-driving-force" model, using the parameters reported by Ptushenko *et al.* (**21**) for the $PhQ_{A/B}$ but considering a larger driving force for F_X oxidation by $F_{A/B}$ (Table 1). The value of the total reorganization energy λ_t was 0.7 eV for all simulations presented in this figure. $[PhQ_A^-(t)]$, dashed-dotted red-line; $[PhQ_B^-(t)]$, dash-dotted blue line; $[F_X^-(t)]$, dash-dotted golden line; $[PhQ_{tot}^-(t)]$, solid black line.

Figure 3. Comparison of the simulations of PhQ^- oxidation kinetics at room temperature (T=290 K) for the "large-driving-force" (**A, C**) and "weak-driving-force" (**B, D**) models, considering different values of total reorganization energy: λ_t = 0.5 eV (**A, B**) and λ_t = 1 eV (**C, D**). All the other parameters as in Table 1 and Figure 1. $[PhQ_A^-(t)]$, dashed-dotted red-line; $[PhQ_B^-(t)]$, dash-dotted blue line; $[F_X^-(t)]$, dash-dotted golden line; $[PhQ_{tot}^-(t)]$, solid black line.

Figure 4. Temperature dependence of the lifetimes associated to PhQ^- oxidation simulated considering the "large-driving-force" configuration. λ_t =1 eV and either $\bar{\omega}_{PhQ \rightarrow F_X} = \bar{\omega}_{F_X \rightarrow F_{A/B}}$ = 150 cm^{-1} (open symbols) or $\bar{\omega}_{PhQ_A \rightarrow F_X}$ = 173 cm^{-1}, $\bar{\omega}_{PhQ_B \rightarrow F_X}$ = 378 cm^{-1} (**31**), and $\bar{\omega}_{F_X \rightarrow F_A}$ = 275 cm^{-1} (closed symbols). The data are compared with the extrapolation of the experimental results from the parameters reported in ref. **31** (**A**) or those which have been scaled to give a closer description of the room temperature values (**C**). Red solid lines: "fast" phase; black solid lines: "slow" phase. The dashed lines represent the confidence interval estimated from a 5% error bound on the parameter estimation of ref. **31** (see text for further details). Lifetimes, τ_1: circles, τ_2: squares, τ_3: diamonds. Panels **B** and **D** shows the results of the simulations and the comparison with the extrapolation of the experimental results in terms of Arrhenius plots.

Figure 5. Temperature dependence of the lifetimes associated to PhQ^- oxidation simulated considering the "weak-driving-force" configuration. λ_t =0.7 eV and either $\bar{\omega}_{PhQ \rightarrow F_X} = \bar{\omega}_{F_X \rightarrow F_{A/B}}$ =150 cm^{-1} (open symbols) or $\bar{\omega}_{PhQ_A \rightarrow F_X}$ = 173 cm^{-1}, $\bar{\omega}_{PhQ_B \rightarrow F_X}$ =378 cm^{-1} (**31**), and $\bar{\omega}_{F_X \rightarrow F_A}$ =275 cm^{-1} (closed symbols). The data are compared with the extrapolation of the experimental results from the parameters reported in ref. **31** (**A**) or those which have been scaled to give a closer description of the room temperature values (**C**). Red solid lines: "fast" phase; black solid lines: "slow" phase. The dashed lines represent the confidence interval estimated from a 5% error bound on the parameter estimation of ref. **31** (see text for further details). Lifetimes, τ_1: circles, τ_2: squares, τ_3: diamonds. Panels **B** and **D** shows the results of the simulations and the comparison with the extrapolation of the experimental results in terms of Arrhenius plots.

Figure 6. Comparison of the simulations of PhQ^- oxidation kinetics at room temperature (T= 290 K) for the "weak-driving-force" model, λ_t =0.7 eV (A) and the "large-driving-force" model, λ_t =1 eV (**B**) with $\bar{\omega}_{PhQ_A \rightarrow F_X}$ = 173 cm^{-1}, $\bar{\omega}_{PhQ_B \rightarrow F_X}$ = 378

cm^{-1} (**31**), and $\bar{\omega}_{F_X \to F_A}$ = 275 cm^{-1} for both energetic scenarios. All other parameters as in Table 1, see text for further detail. $[PhQ_A^-(t)]$, dashed-dotted red-line; $[PhQ_B^-(t)]$, dash-dotted blue line; $[F_X^-(t)]$, dash-dotted golden line; $[PhQ_{tot}^-(t)]$, solid black line.

Figures.

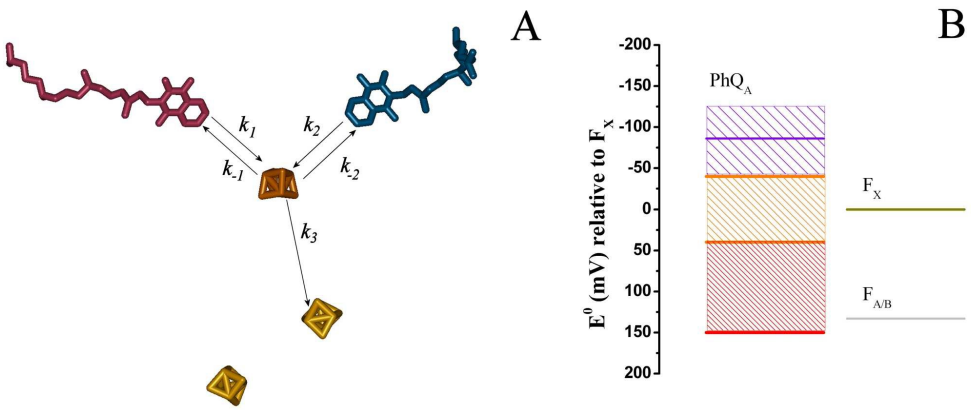

Figure 1

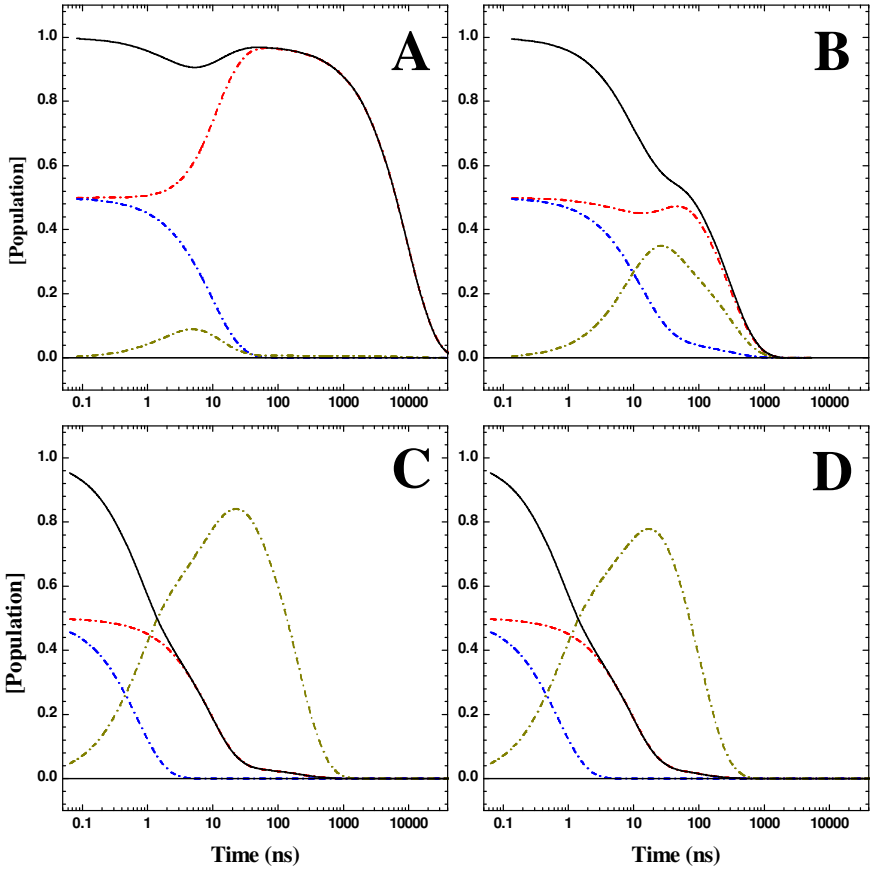

Figure 2

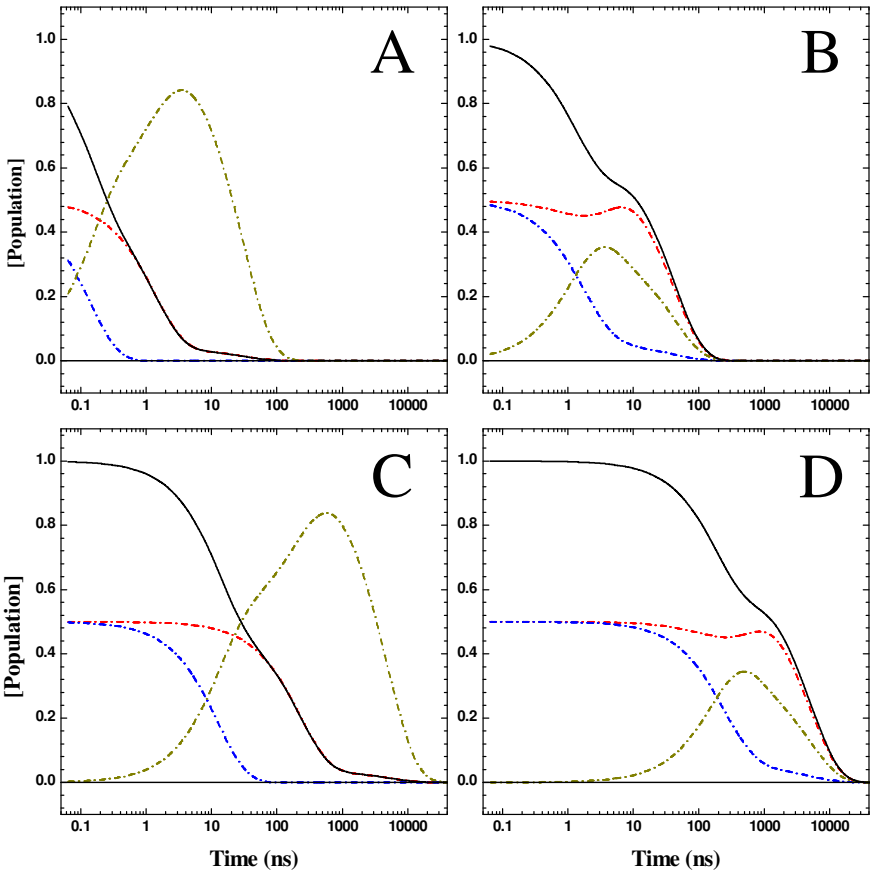

Figure 3

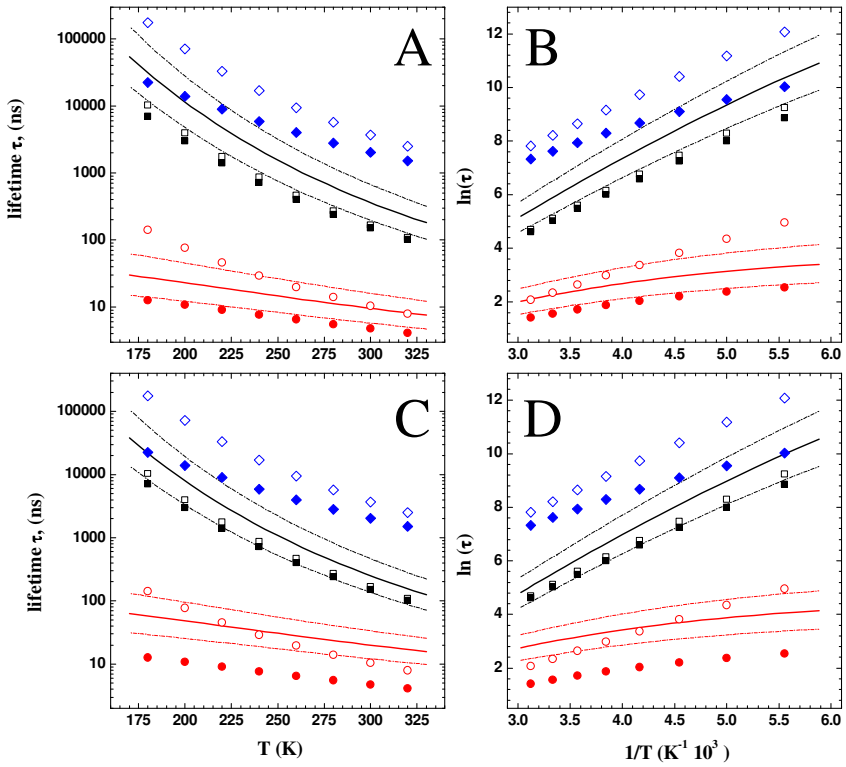

Figure 4

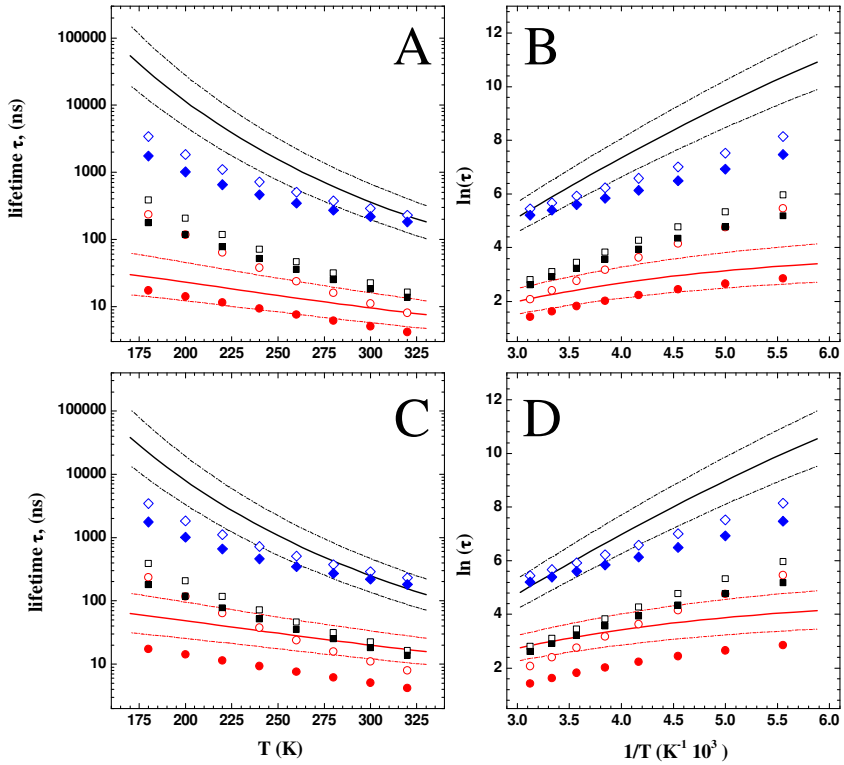

Figure 5

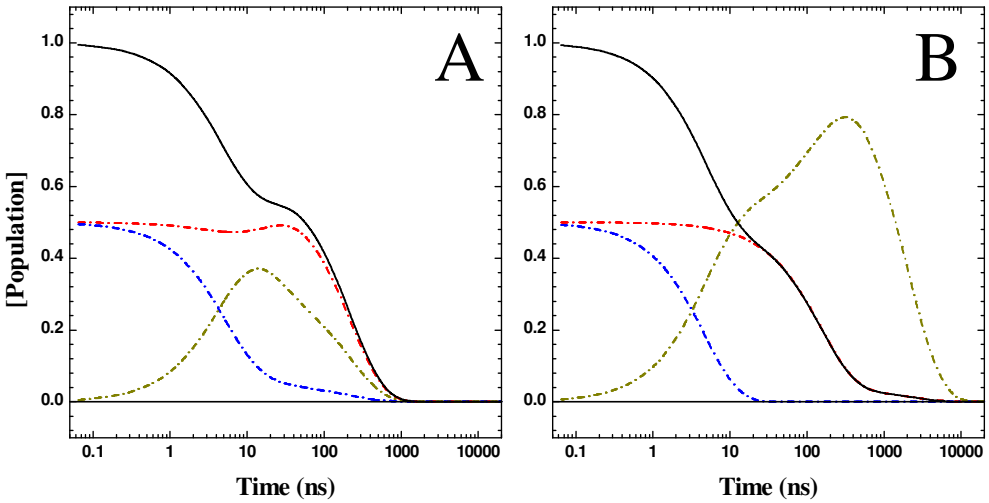

Figure 6

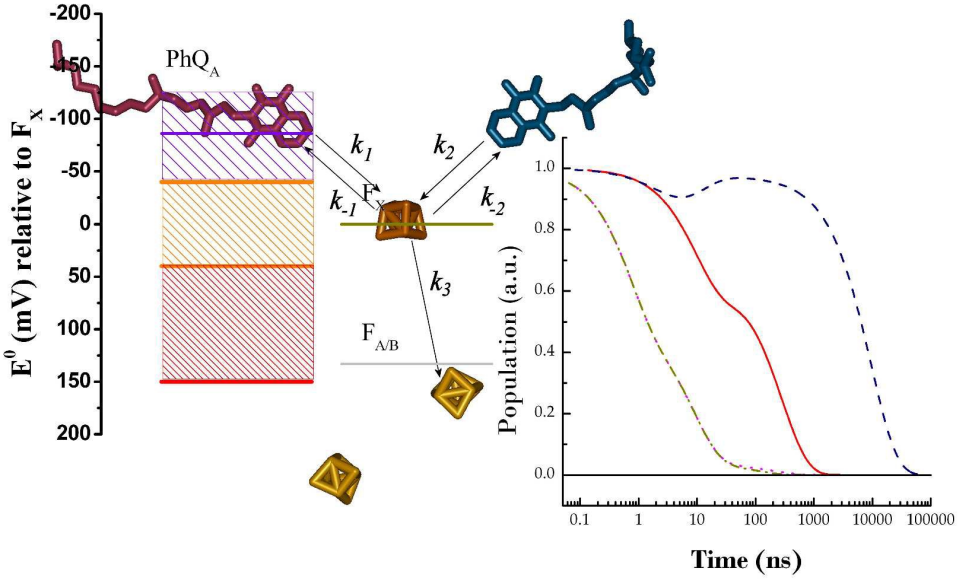

T.O.C. Image.